Electronic Supplementary Material (ESI) for Physical Chemistry Chemical Physics.

Supplementary Information

Selective formation of molecular junctions with high and low conductance states by tuning the velocity of electrode displacement

Yuji Isshiki,[a] Shintaro Fujii,[a] Tomoaki Nishino[a] and Manabu Kiguchi[a]

[a]Department of Chemistry, Graduate School of Science and Engineering, Tokyo Institute of Technology,
2-12-1 W4-10 Ookayama, Meguro-ku, Tokyo 152-8551

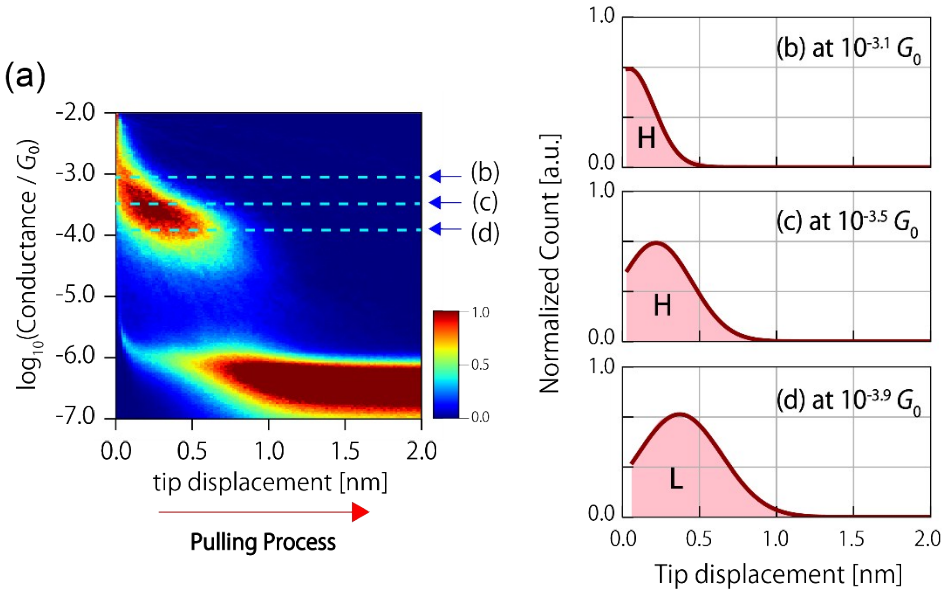

Fig. S1 (a) 2D histogram of the conductance versus tip displacement curve measured at the velocity of electrode displacement (v) = 16 nm/s in the pulling process (see Fig. 2a). Tip displacement is defined as the displacement from the tip position at the conductance of 0.014 G_0. Dashed lines in (a) correspond to conductance values of $10^{-3.1}$, $10^{-3.5}$, and $10^{-3.9}G_0$ respectively. (b-d) Tip displacement histograms within conductance windows of $10^{-3.1\pm0.01}$, $10^{-3.5\pm0.01}$, and $10^{-3.9\pm0.01}$ G_0. Tip displacement is defined as the relative distance from a reference position where the conductance became 1.4×10^{-2} G_0 ($G_0 = 2e^2/h \sim 77.45\ \mu/\Omega$).

1. Conductance behaviour and histogram fitting in Fig. 2c,e

It has been demonstrated that pyridine-based analogue molecules such as pyrazine, 4,4'-bipyridine (BPY), and 1,4-di(4-pyridyl)benzene (DPB) showed two junction-conductance (*i.e.*, high and low conductance) in the junction pulling process.[1-3] The junction conductance of pyridine-based of the pyridine-based analogue molecules was mainly influenced by molecular orientation in the junctions.[1-3] The molecular orientation correlates with the molecule-electrode electric coupling and the junction conductance. When a pyridine-based molecule adopts a tilted orientation in a junction, π-electron in a pyridine ring interact with an electrode, which induces higher electric coupling and junction conductance than those of a molecule with an upright orientation. Quek *et al*. fabricated a pyridine-based molecular junction of BPY in the pulling process of the junction and found that a mechanical compression and elongation of the pyridine-based molecular junction can induce change between the above-mentioned molecular orientations and the corresponding junction conductance. This finding was supported by theoretical simulations,[1] in which rotation of adjacent aromatic rings in BPY was not main response to the mechanical perturbation. In a similar manner to BPY, the conductance change observed for the DPB-molecule junctions in the pulling process (Fig. 2a) was most probably due to the change in the molecular orientation in the junction. The analysis in the *I*−*V* curves of DPB in the pushing process revealed that the high and low states showed similar ε (ε = 1.0 and 0.9 eV (Table 1)). These results suggested that two independent metal-molecule interface structures with substantial differences in electric coupling (Γ = 23 and 13 meV (Table 1)) formed in the pushing process of DPB. It has been reported that rotation of adjacent aromatic rings from the planar structure increases the HOMO-LUMO gap for biphenyl derivatives. For example, a HOMO-LUMO gap of biphenyl (*i.e.*, phenylbenzene) increases by *ca*. 1 eV in a change of the dihedral angle from 0° to 90°.[4] In the present study, the high and low state of DPB showed similar ε (ε = 1.0 and 0.9 eV (Table 1)) and therefore have similar rotation of aromatic rings.

Fig. 2e in the main text shows the conductance histogram for the pulling process of the DPB-single-molecule junctions. As described above, the pyridine-based analogue molecules show two junction conductance (*i.e.*, high and low conductance)[1-3] and also the analysis in the probable displacements of the junction electrode suggests that two conductance states are present (Fig. 2c, for a detail see main text). Therefore, the conductance histogram in Fig. 2e was fitted by multiple Gaussian distributions ($n \geq 2$, n is numbers of Gaussian distributions) as shown in Fig. S2 and Table S1. For n = 2, contribution of each fitted distribution to the total one was 18% and 82% (Table S1). For n = 3, contribution of each fitted distribution to the total one was 14%, 85%, and 1% in descending order in their peak values (Table S1). The contribution of the third peak is as small as 1% and is negligible for the triple Gaussian fitting (n = 3). Therefore, the conductance histogram in the main text (Fig. 2e) is fitted by the double Gaussian (n = 2).

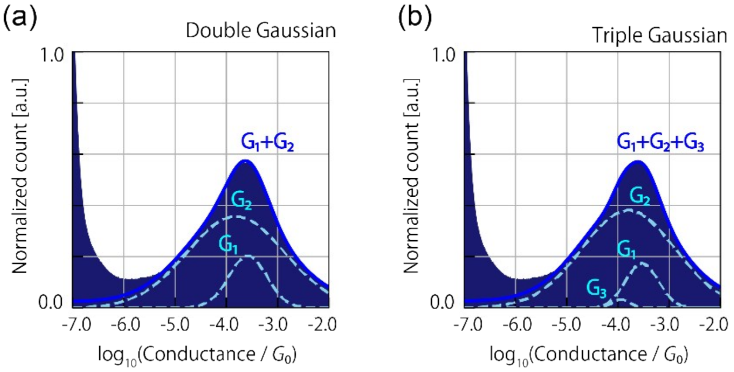

Fig. S2 (a,b) Conductance histograms in the pulling process fitted with (a) double, and (b) triple Gaussian curves. Conductance range used for the fitting was from 10^{-5} to 10^{-2} G_0.

	G /mG_0	Contribution*
(a) Double Gaussian	(Peak 1) 0.26	18%
	(Peak 2) 0.16	82%
(b) Triple Gaussian	(Peak 1) 0.29	14%
	(Peak 2) 0.16	85%
	(Peak 3) 0.11	1%

Table S1 Peak conductance and contribution of the multiple Gaussian distributions for the histogram fitting in Fig. S2. * Contribution of each Gaussian distribution to the total distribution

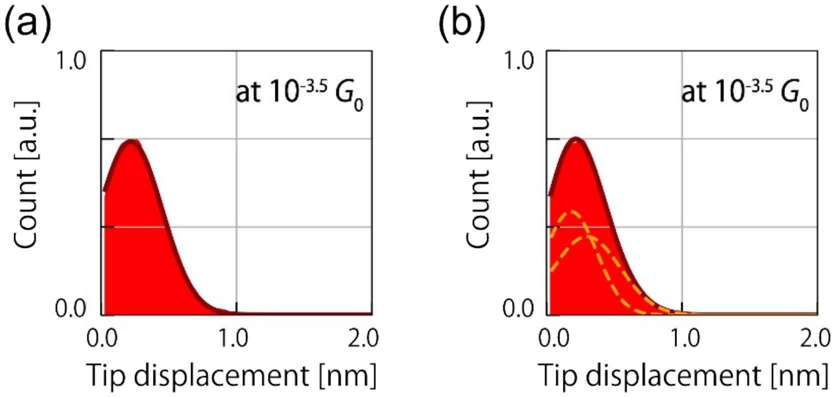

Fig. S3 Tip displacement histograms for the conductance window of $10^{3.5\pm0.01}G_0$ (See Fig. S1c) and fitted curves with (a) single and (b) double Gaussian curve(s).

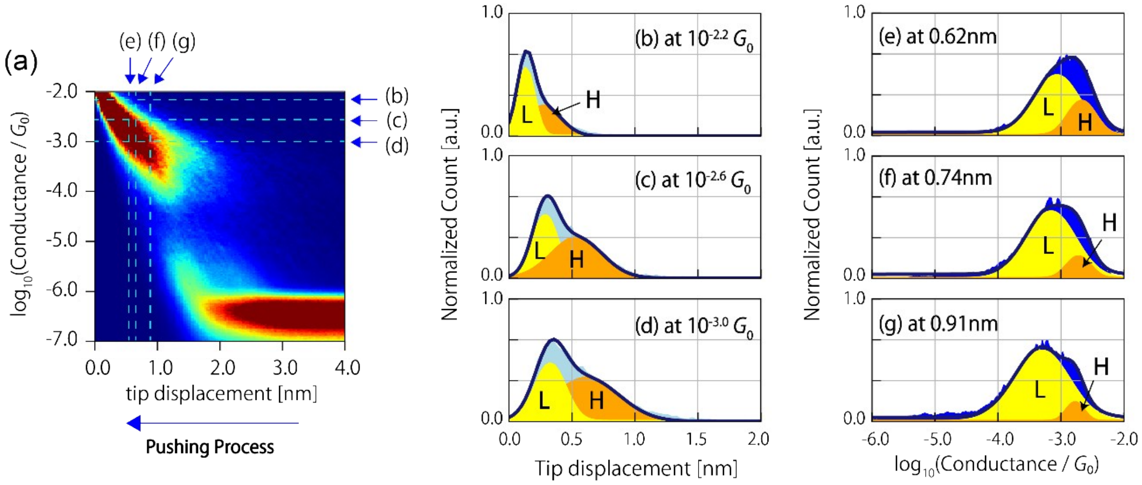

Fig. S4 (a) 2D histogram of conductance versus tip displacement curves for the pushing process (see Fig. 2b). Dashed horizontal lines correspond to conductance values of $10^{-2.2}$, $10^{-2.6}$, and $10^{-3.0}$ G_0 respectively. Dashed vertical lines correspond to tip displacement values of 0.62, 0.74, and 0.91 nm. (b–d) Tip placement histograms constructed from data in conductance windows of $10^{-2.2\pm0.01}$, $10^{-2.6\pm0.01}$, and $10^{-3.0\pm0.01}G_0$. (e–g) Conductance histograms constructed from data in tip-displacement-windows of 0.62±0.0162, 0.74±0.0162, and 0.91±0.0162 nm.

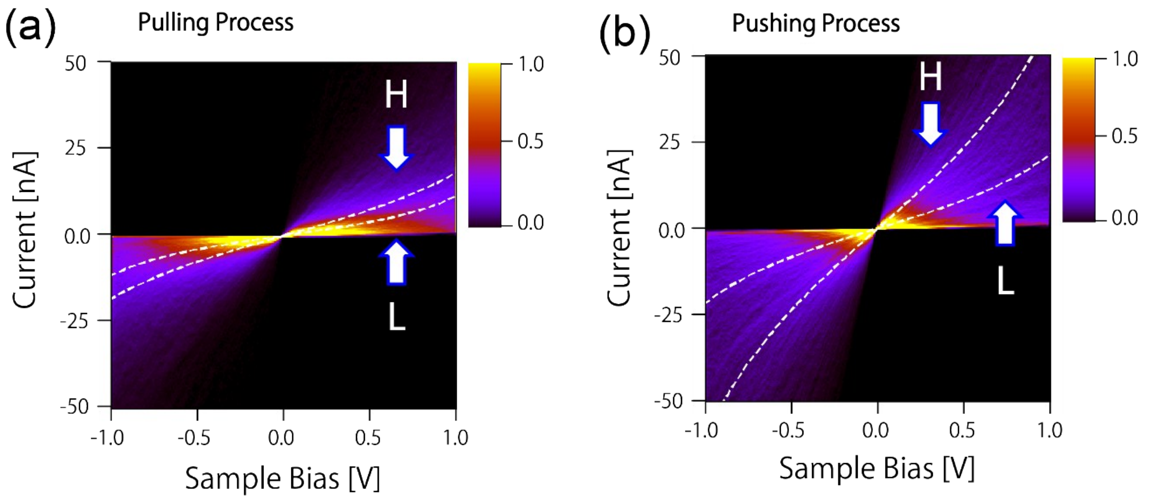

Fig. S5 2D histograms of the current versus voltage curves measured in the (a) pulling process and (b) pushing process. White dashed lines show theoretical *I*–*V* curves obtained using equation (1) in the Results and Discussion section in the paper, and the most probable values of ε and Γ determined in Fig. 3 (see also Table 1).

2. *I–V* Fitting based on the single level model

Within the single channel transport model, the transmission probability of a single-molecule junction can be represented by

$$\tau(E)=\frac{4\Gamma_L\Gamma_R}{(\Gamma_L+\Gamma_R)^2+(E-\varepsilon_0)^2} \tag{SI-1}$$

where ε_0 and $\Gamma_{\mathrm{L(R)}}$ are the energy of the conduction orbital and the electronic coupling energy between the molecule and the left (right) electrode, respectively. Here, we set the Fermi level, E_{F}, to zero. The current through the molecular junction is expressed by

$$I(V)=n\int dE\tau(E)\left\{f\left(E-\frac{eV}{2},T\right)-f\left(E+\frac{eV}{2},T\right)\right\} \tag{SI-2}$$

where n is the number of bridging molecules and f is the Fermi distribution function. When the electronic temperature, T, is set to 0 K, equation (SI-2) can be analytically evaluated as

$$I(V)=n\frac{8e}{h}\alpha(1-\alpha)\Gamma\left\{\arctan\left(\frac{\alpha eV-\varepsilon_0}{\Gamma}\right)+\arctan\left(\frac{(1-\alpha)eV+\varepsilon_0}{\Gamma}\right)\right\} \tag{SI-3}$$

where $\Gamma=\Gamma_{\mathrm{L}}+\Gamma_{\mathrm{R}}$ and $\alpha=\Gamma_{\mathrm{L}}/\Gamma$.[3,5–7]

Fig. S6 show histograms of the number of bridging molecules (n), which is obtained by fitting *I–V* curves in the H and L states (Fig. 3b) using equation (SI-3). The histograms revealed that more than 94 % of the junctions consisted of a single molecule (n = 1). Therefore, the *I–V* fitting in the main text was performed under the constraint condition of n =1. Fig. S7a,b show histograms of ε and Γ values for the above-mentioned 94 % of the junctions (n = 1). Fig. 6c,d show histograms of ε and Γ values, which are obtained by fitting all *I–V* curves in the pushing process using equation (SI-3) under the constraint condition of n =1. We confirmed that the *I–V* fitting with and without the constraint condition showed almost the same results (see Fig. S7c,d and Fig. S7a,b).

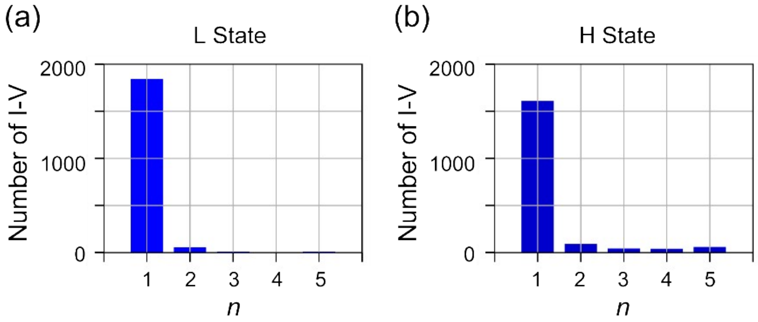

Fig. S6 Histograms of the number of bridging molecules (*n*), which are obtained by fitting the *I*–*V* curves in the H and L states (Fig. 3b) using equation (SI-3).

	n = 1	n = 2	n = 3	n = 4	n = 5
H State	1608	91	42	40	60
L State	1845	56	11	2	9

Table S2 Number of fitted *I*–*V* curves for *n* = 1, 2, 3, 4, and 5 for the H and L states.

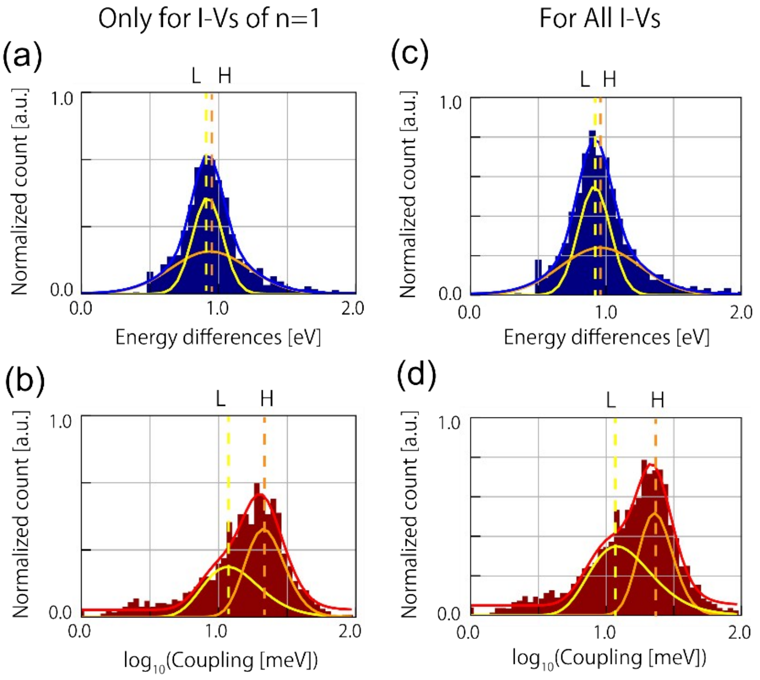

Fig. S7 (a,b) Histograms of *ε* and *Γ* values for the *I*–*V* curves of *n* = 1 in the pushing process. (c,d) Histograms of *ε* and *Γ* values, which are obtained by fitting all *I*–*V* curves in the pushing process using equation (3) under constraint condition of *n* = 1.

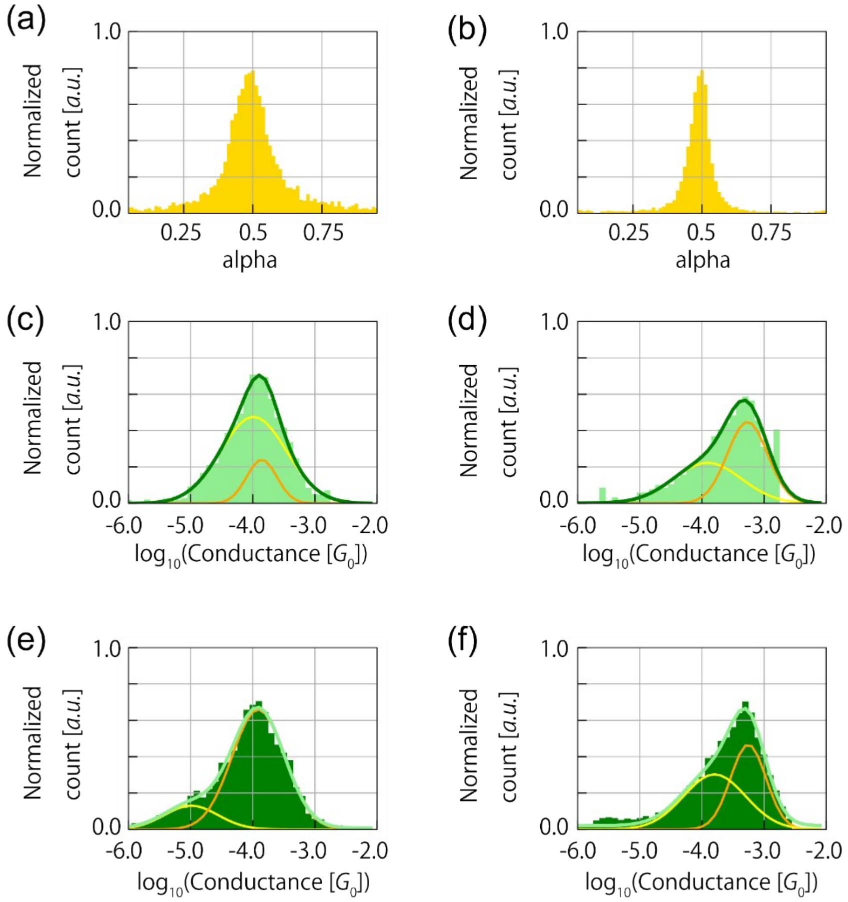

Fig. S8 (a,b) Histograms of the symmetric parameter α for the (a) pulling and (b) pushing processes. (c,d) Zero bias conductance histograms, in which conductance is calculated by Γ and ε values using equation (SI-1) in Supplementary Information 1. The Γ and ε values are obtained by fitting each *I*−*V* curve in Fig. 3a,b. (e,f) Conductance histograms obtained by dividing the current by the bias voltage in a bias range from 75 mV to 125 mV in each *I*−*V* curve in Fig. 3a,b.

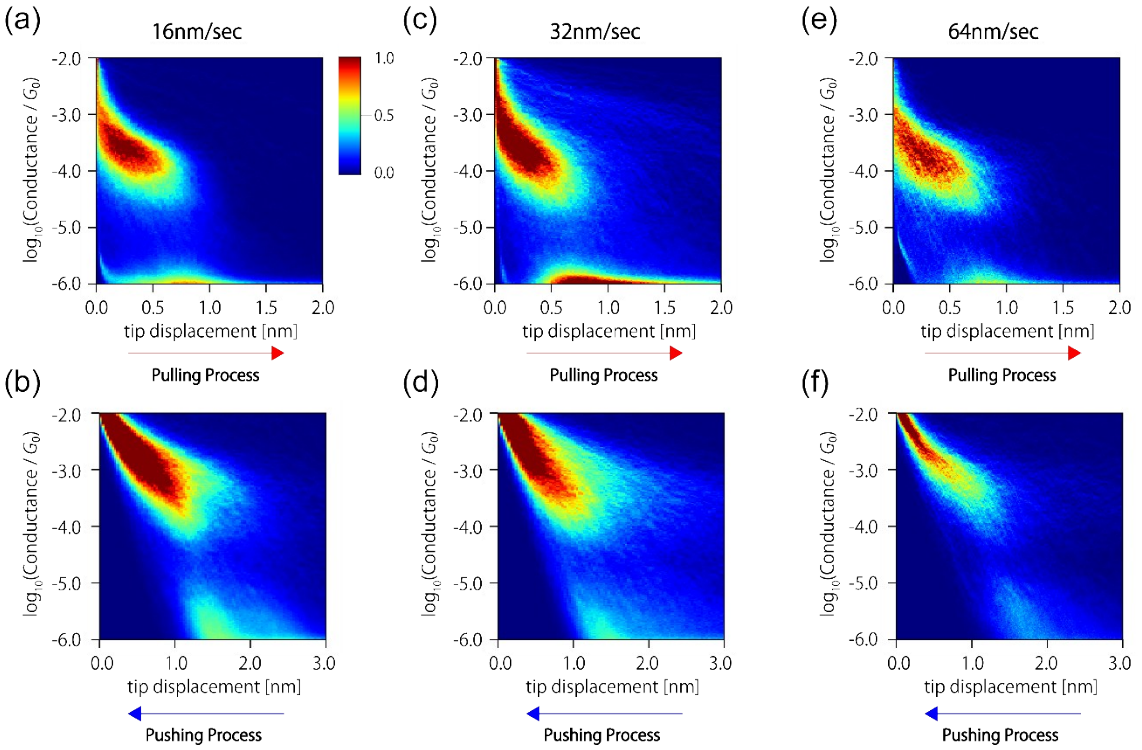

Fig. S9 (a-f) 2D histograms of the conductance versus tip displacement for (a,c,e) the pulling and for (b,d,f) the pushing process. The histograms were constructed form the data measured at the velocity of tip displacement of (a,b) 16 nm/s, (c,d) 32 nm/s, and (e,f) 64 nm/s.

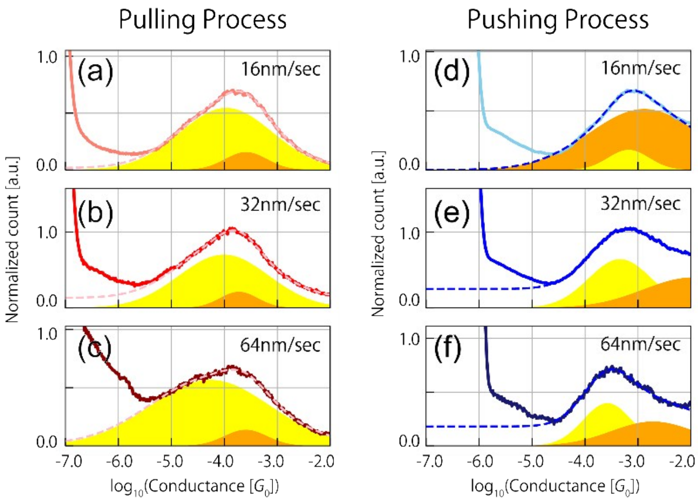

Fig. S10 (a-f) Conductance histograms at different speeds of tip displacement (a-c) in pulling and (d-f) in pushing process. Histograms of high and low conductance states were respectively coloured by orange and yellow, and the dashed lines are the sum of high and low conductance histograms.

3. DFT simulation of the DPB junction

DFT calculation of the DPB-single-molecule junctions sandwiched by two Au electrodes was conducted using cluster models where each side of the junction consists of 74 Au atoms. During geometrical optimization, the two outer double Au layers of the left and right electrodes were fixed, and the other atomic positions were allowed degrees of freedom. All calculations were performed using the Perdew–Burke–Ernzerhof XC functional.[8,9] The electronic wave functions were expanded in a double-numeric polarized basis set with a real-space cutoff of 0.4 nm using Dmol3 code.[10,11] We used the method of dispersion correction as an add-on to standard the Kohn–Sham density functional theory (DFT-D).[12] We determined the initial atomic coordinates of molecular junctions as follows: First, the optimized geometrical structure of isolated molecules was calculated. Secondly the geometry of a pyramidal Au cluster consisting of 74 Au atoms was optimized. Next, the Au cluster was attached to the relaxed DPB molecule and optimized again. In this optimization, the bottom double layer of the Au cluster was fixed and the top layer was relaxed, and furthermore the DPB molecule was attached on a Au atom at A-top position. After optimization of this DPB-Au junction, the DPB molecule was tilted by 10° to be parallel to the Au surface and optimized again. Here, we tilted DPB along the direction from vector N-N to vector Au in Fig. S11. We repeatedly optimized the configuration of the DPB-Au junction with 8 different angles between the gold surface and the N vector (Fig. S11). Finally, Au-DPB-Au junction structures with two Au clusters were constructed by adding another Au cluster to the 2nd relaxed geometry using mirror symmetry at the molecular centre.

To quantitatively evaluate the influence on the LUMO energy by conformational changes of our DPB-Au junction, we optimized the most probable Au-DPB-Au junction at the angle of 3.7°, and the junction at the angle of 69.1° (Fig. S11(a-1), (a-2)). Next, to include the influence on LUMO energy by site change of the DPB-Au interface, we shifted the position of the Au cluster, as in Fig. S12(b), by 0.1 nm along the Au vector. The LUMO energies of each structure were −2.293 eV for (a), −2.388 eV for (b), and −2.413 eV for (c). Our *I*–*V* measurements show that the LUMO energies of H and L states in the pushing process all have only a 10% difference, while in the pulling process, the difference in LUMO energies between H and L states is around 30%. Therefore, our calculation and experimental data imply that one of the possible variables in determining the geometric differences between H and L states is the adsorption site of DPB on the Au surface.

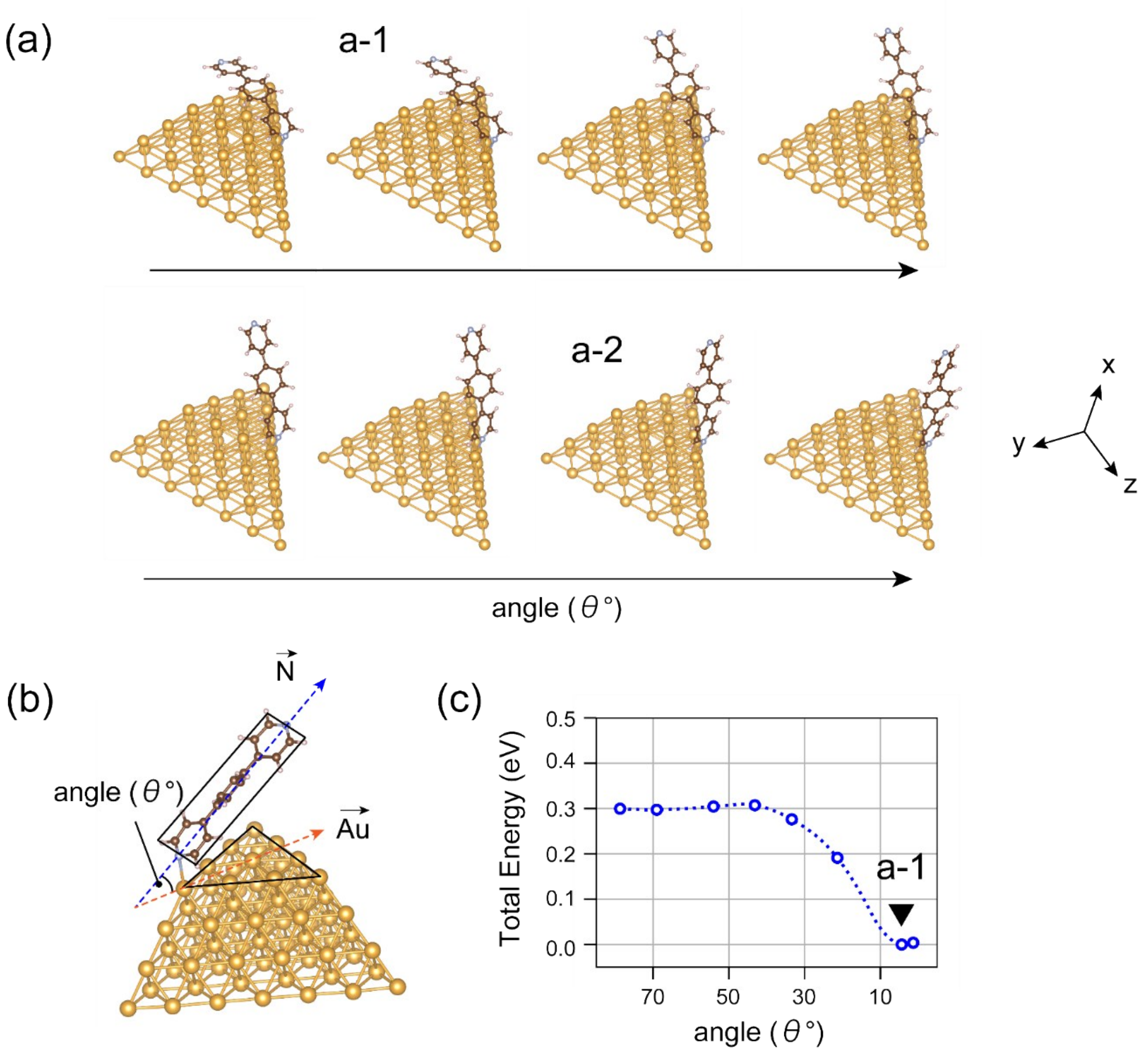

Fig. S11 (a) Optimized geometries of DPB-Au junctions with different angles. (b) Definition of the positions of vector $\vec{N}$, vector $\vec{Au}$, and angle (θ). (c) Calculated total energy of DPB-Au junctions as a function of the angle between $\vec{N}$ and $\vec{Au}$. Here, the total energies are shown as the relative value of energy at the angle of 3.7°.

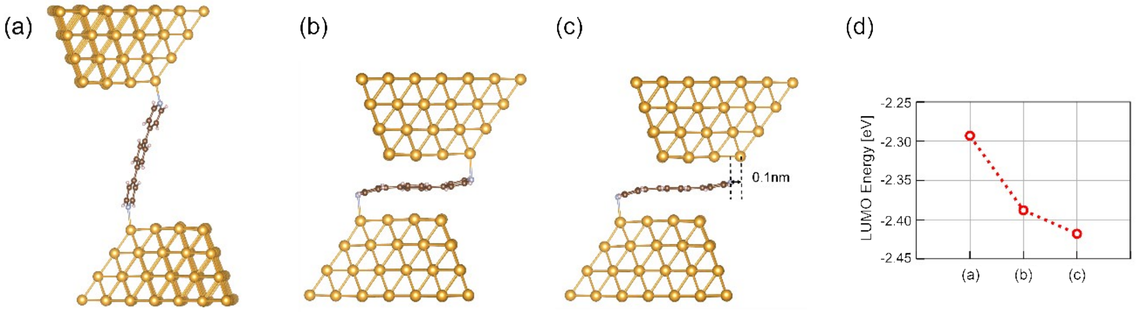

Fig. S12 (a-b) Optimized geometries of Au-DPB-Au junctions with different angles between $\vec{N}$ and $\vec{Au}$: (a) 69.1° and (b) 3.7°. (c) Optimized geometry of a Au-DPB-Au junction with mismatched contacts between DPB and the Au cluster. (d) LUMO energy of the Au-DPB-Au junctions in (a-c).

References

1. S. Y. Quek, M. Kamenetska, M. Steigerwald, H. J. Choi, S. G. Louie, M. S. Hybertsen, J. B. Neaton, L. Venkataraman, *Nat. Nanotech.*, 2009, **4**, 230–234.
2. M. Kamenetska, S. Y. Quek, A. C. Whalley, M. L. Steigerwald, H. J. Choi, S. G. Louie, C. Nuckolls, M. S. Hybertsen, J. B. Neaton, L. Venkataraman, *J. Am. Chem. Soc.*, 2010, **132**, 19, 6817–6821.
3. Y. Isshiki, S. Fujii, T. Nishino and M. Kiguchi, *J. Am. Chem. Soc.*, 2018, **140**, 3760−3767.
4. L. Zhang, M. Ye, L. Zheng, H. Li, Y. Li, X. Fan, *Compt. Thor. Chem.*, 2016, **1085**,1−6.
5. E.-D. F. A. Borges, Fay Ng, L. Venkataraman and Gemma C. Solomon, *J. Phys. Chem. Lett.*, 2016, **7**, 4825−4829.
6. Y. Komoto, S. Fujii, H. Nakamura, T. Tada, T. Nishino and M. Kiguchi, *Sci. Rep.*, 2016, **6**, 26606.
7. Y. Komoto, Y. Isshiki, S. Fujii, T. Nishino and M. Kiguchi, *Chem. Asian. J.*, 2017, **12**, 440−445.
8. J. P. Perdew, K. Burke and M. Ernzerhof, *Phys. Rev. Lett.*, 1996, **77**, 3865−3868.
9. J. P. Perdew, M. Ernzerhof and K. Burke, *J. Chem. Phys.*, 1996, **105**, 9982−9985.
10. B. Delley, *J. Chem. Phys.*, 1990, **92**, 508−517.
11. B. Delley, *J. Chem. Phys.*, 2000, **113**, 7756−7764.
12. S. Grimme, *WIREs Comp. Mol. Sci.*, 2011, **1**, 211−228.